

The Characterisation of Supported Platinum Nanoparticles on Carbon Used for Enantioselective Hydrogenation: A Combined Electrochemical – STM Approach

Gary A. Attard,^{*,[a]} Ahmad Ahmadi,^[a] David J. Jenkins,^[a] Omar A. Hazzazi,^[a] Peter B. Wells,^[a] Ken G. Griffin,^[b] Peter Johnston,^[b] and Jennifer E. Gillies^[b]

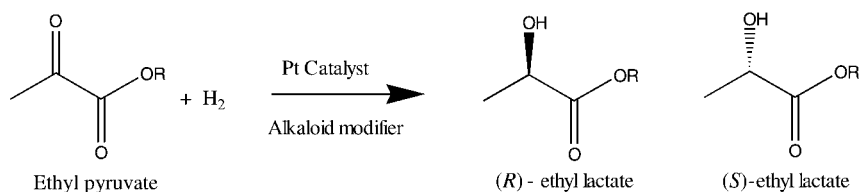
The action of chiral modifiers like cinchonine and cinchonidine in facilitating enantioselectivity in heterogeneous catalysis is investigated using a combination of electrochemical and scanning probe methods. The surface chirality of corner kink sites is suggested as being crucial for chirality recognition at supported

catalyst nanoparticles. Other aspects of chirality in relation to one, two, three and four dimensions are also discussed.

KEYWORDS:

catalysis · cyclic voltammetry · electrochemistry · enantioselectivity · nanoparticles · scanning probe microscopy · surface chirality

The ability of surface chemists to control and characterise both the distribution and nature of active sites across a supported metal nanoparticle lies at the heart of new developments in surface catalysis and electrocatalysis. Of particular concern is the identification of enantioselective surface catalytic sites, since their generation offers a means of mass producing chiral materials heterogeneously without the need of, for example, expensive phase separations of the homogeneous catalyst from the reaction mixture. When it is realised that the pharmaceutical industry alone is worth some $\text{£}100 \times 10^9$ ($\text{€}170 \times 10^9$) a year,^[1] not only does *chirality in two dimensions* become a fascinating problem in surface science, but also one in which a significant impact on a company's balance sheet could be realised by the invention of the appropriate enantioselective supported catalyst. It has recently been demonstrated using the electro-oxidation of D- and L-glucose that metal kink sites are intrinsically chiral,^[2–5] and hence supported heterogeneous metal catalysts may be thought of as racemates containing a 50:50 distribution of left- and right-handed kink sites.^[5] In this context, enantioselectivity may be considered as arising from the selective blocking or generation of such sites at the catalyst surface. However, for one of the most studied of these types of reactions, namely the enantioselective hydrogenation of methyl and ethyl pyruvate over cinchona-modified supported platinum (Scheme 1; the "Orito" reaction^[6–14]), it appears that indiscriminate adsorption of the chiral cinchona modifier takes place, at least in the absence of the other reactants such as hydrogen, solvent and ethyl pyruvate,^[5] and that the chemisorbed cinchona adlayer itself is disordered under ultrahigh vacuum (UHV)



Scheme 1. The Orito reaction: Enantioselective hydrogenation of pyruvates over an alkaloid-modified Pt catalyst.

conditions.^[14] Hence these findings appear to negate any role for chiral surface defects during the Orito reaction.^[5,15] Nonetheless, there are reported to be important structural aspects to enantioselection based on particle size effects^[16] and in fact, from fundamental surface science studies of single crystal surfaces, for many heterogeneous catalytic reactions, structure sensitivity is predicted.^[17] Hence there is a pressing need to identify "active sites" on supported nanoparticles at a local, molecular level.

Electrochemical techniques of surface characterisation may offer several advantages over more traditional methods based

[a] Prof. G. A. Attard, Dr. A. Ahmadi, D. J. Jenkins, O. A. Hazzazi, Prof. P. B. Wells
Department of Chemistry
Cardiff University
P.O. Box 912, Cardiff CF10 3TB (UK)
Fax: (+44) 29-2087-4030
E-mail: attard@cardiff.ac.uk

[b] K. G. Griffin, Dr. P. Johnston, J. E. Gillies
Johnson Matthey
Orchard Road
Royston SG8 5HE (UK)

on single crystal, UHV and electron-based spectroscopic approaches.^[18] The most important of these would be the direct surface interrogation of "real" supported catalysts under ambient pressure and reaction conditions, that is, the bridging of the so-called "pressure" and "materials" gap between surface science and heterogeneous catalysis. In this report, the possibility of using cyclic voltammetry (CV) in conjunction with scanning tunnelling microscopy (STM) to characterise the surface morphology of supported platinum nanoparticles is expounded. That CV is a structural probe of local surface structure has been confirmed over the last twenty years or so using well-defined single crystal electrodes.^[19] Moreover it continues to play an important role in quantifying electrocatalytic activity and selectivity in many important reactions including the hydrogen- and methanol-based fuel cell reactions.^[19]

Figure 1 shows CVs from a variety of single crystal platinum surfaces and the corresponding surface adsorption sites giving rise to the individual voltammetric features observed. A general finding from such studies is that widely spaced (> 6 atomic rows on average) linear step sites give rise to very sharp step voltammetric features. These features broaden considerably when the average terrace width begins to diminish and/or kink sites associated with the intersection of two linear steps are

present. Hence, the CV is sensitive to both the local surface morphology of the single crystal surface and also the surface density of step and terrace adsorption sites via the relative intensities of the corresponding voltammetric peaks. This means that for platinum nanoparticles > 7 nm in diameter (when the electronic properties of the particle are closely similar to the bulk metal) the absence or presence of such sites may be discerned from a simple electrochemical measurement. However, this approach can be taken one stage further. Recent electrochemical studies have shown that many adsorbates bond irreversibly to platinum single crystal surfaces in a site-selective manner.^[20–24] Hence deposition of adatoms onto supported platinum nanoparticles should proceed in a similar way. Figure 2 shows the adsorption of bismuth adatoms onto Pt(332) [average (111) terrace width = 6 Pt atoms separated by $(111) \times (111)$ linear steps] and Pt(11,1,1) [average (100) terrace width = 6 Pt atoms but separated by $(111) \times (100)$ linear steps]. The presence of the bismuth in both cases manifests itself as a diminution of intensity in the potential range 0–0.5 V and, for Pt(332), the appearance of a bismuth surface redox peak at 0.58 V at highest coverage associated with bismuth adsorption on (111) terraces.^[20, 21] It should be noted that for Pt(332) the step site is attenuated first of all followed by the (111) terrace site. In contrast, for Pt(11,1,1) the much more corrugated nature of the

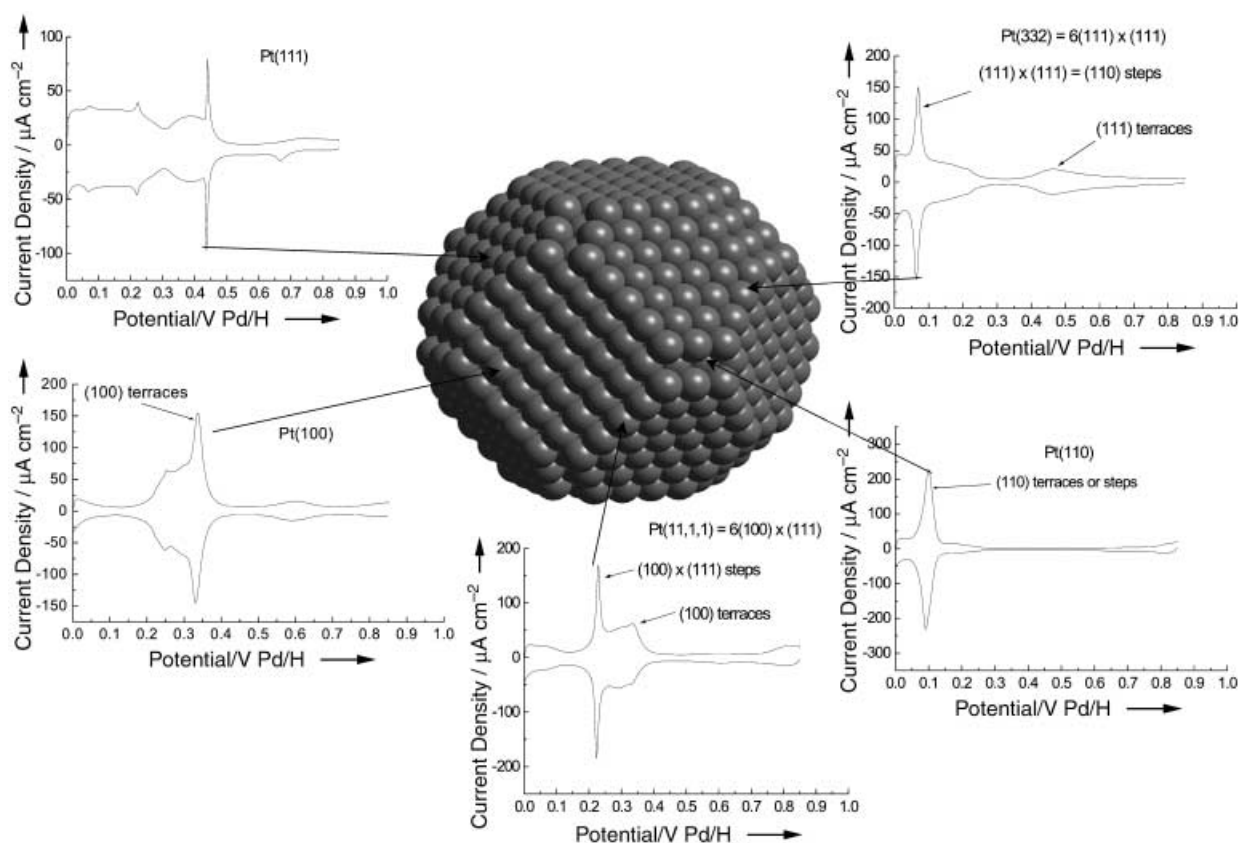


Figure 1. CV data from a variety of single crystal Pt electrodes in 0.1 M sulphuric acid collected at a sweep rate of 50 mVs^{-1} . The various voltammetric electrodesorption peaks observed are associated with particular fundamental adsorption sites and these are indicated in relation to a model cubo-octahedral Pt nanocrystal. For nanoparticles $> 2\text{--}3$ nm in diameter, such as might be used in an enantioselective hydrogenation, it is possible to use voltammetry to identify both the nature and population of these sites at the catalyst surface.

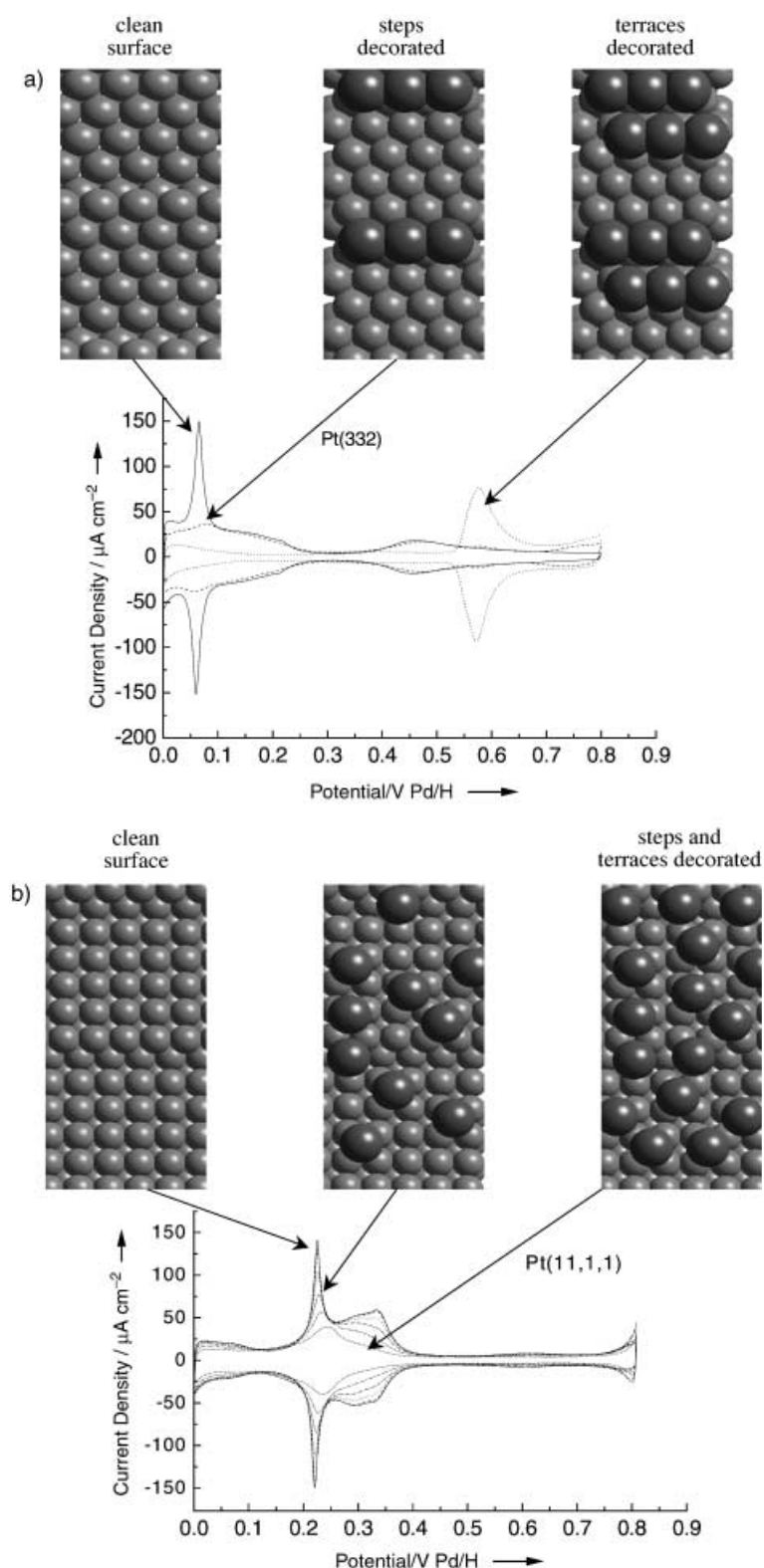


Figure 2. The surface sites highlighted in Figure 1 may also be decorated with foreign adatoms to form bimetallic surfaces. In this Figure, the changes in voltammetry for Bi adsorption on a) Pt(332) and b) Pt(11,1,1) are reported. For Pt(332), rapid surface diffusion of bismuth adatoms on close-packed (111) terraces ensures that the step sites are decorated preferentially as signified by the attenuation of the (110) step electroadsorption peak prior to adsorption at (111) terrace sites. In contrast, the more open (100) terrace sites of Pt(11,1,1) give rise to a slower rate of surface diffusion and simultaneous blocking of terrace and step sites as shown by simultaneous attenuation of all electroadsorption features as a function of Bi loading.

more open (100) terrace sites hinders surface diffusion and causes nucleation and growth of bismuth simultaneously at terrace and step sites as indicated by the attenuation of all voltammetric terrace and step peaks. When bismuth is adsorbed onto a supported Pt catalyst, it should be expected therefore that the defect and (100) terrace sites should be blocked before the (111) terrace sites. This is indeed found to be the case as shown in Figure 3. Hence if either the (111) terrace sites or defect sites are postulated as being active sites in a particular heterogeneous reaction, it may be possible by electrochemical means not only to determine the surface coverage of "free" Pt sites (ratio of voltammetric peak intensity of the clean versus the modified surfaces) but also to state the occupancy of individual surface sites by the adatom. Hence using such well-defined supported catalysts blocked with chemically inactive adatoms, it is possible to relate surface activity and selectivity directly to fundamental adsorption sites on the catalyst.

Heat treatments of supported catalysts may also be used to engender structural transformations in the supported particle that in turn may be followed by cyclic voltammetry.^[25] For example, Figure 4 shows TEM data for a 5% Pt/graphite catalyst together with data for the same catalyst after annealing for several hours in argon at 400, 600, 700 and 800 K. It is evident that annealing leads to "de-necking" of the catalyst particles. At 400 K, the de-necking commences and the extent of agglomeration is reduced. By 600 K, all the particles are de-necked with substantial particle growth appearing together with some particle faceting (some straight edges appear together with "hexagonal" particles). At 700 K virtually all particles are faceted and by 800 K the fraction of small particles is markedly reduced. The CVs of the unannealed and heat-treated (700 K) catalyst, normalised to about the same hydrogen peak area, are shown in Figure 4. Of course the real surface area of the 700 K catalyst is small relative to the unannealed catalyst due to sintering and hence the total area under the voltammetric peaks is also smaller. It is clear that the main transformations in the form of the CV after annealing are that (100) terrace sites are much attenuated, that (111) terraces are more extended and abundant (shift of voltammetric peak to more negative potentials and relatively increased intensity^[19]) and that (111) \times (111) step defect peaks are slightly narrower. These results would be consistent with the TEM data if the necking regions were mostly composed of (100) terraces and the faceting corresponded to a lengthening of straight regions of the particle/support perimeter. To gain further information concerning how straight are the edges of the

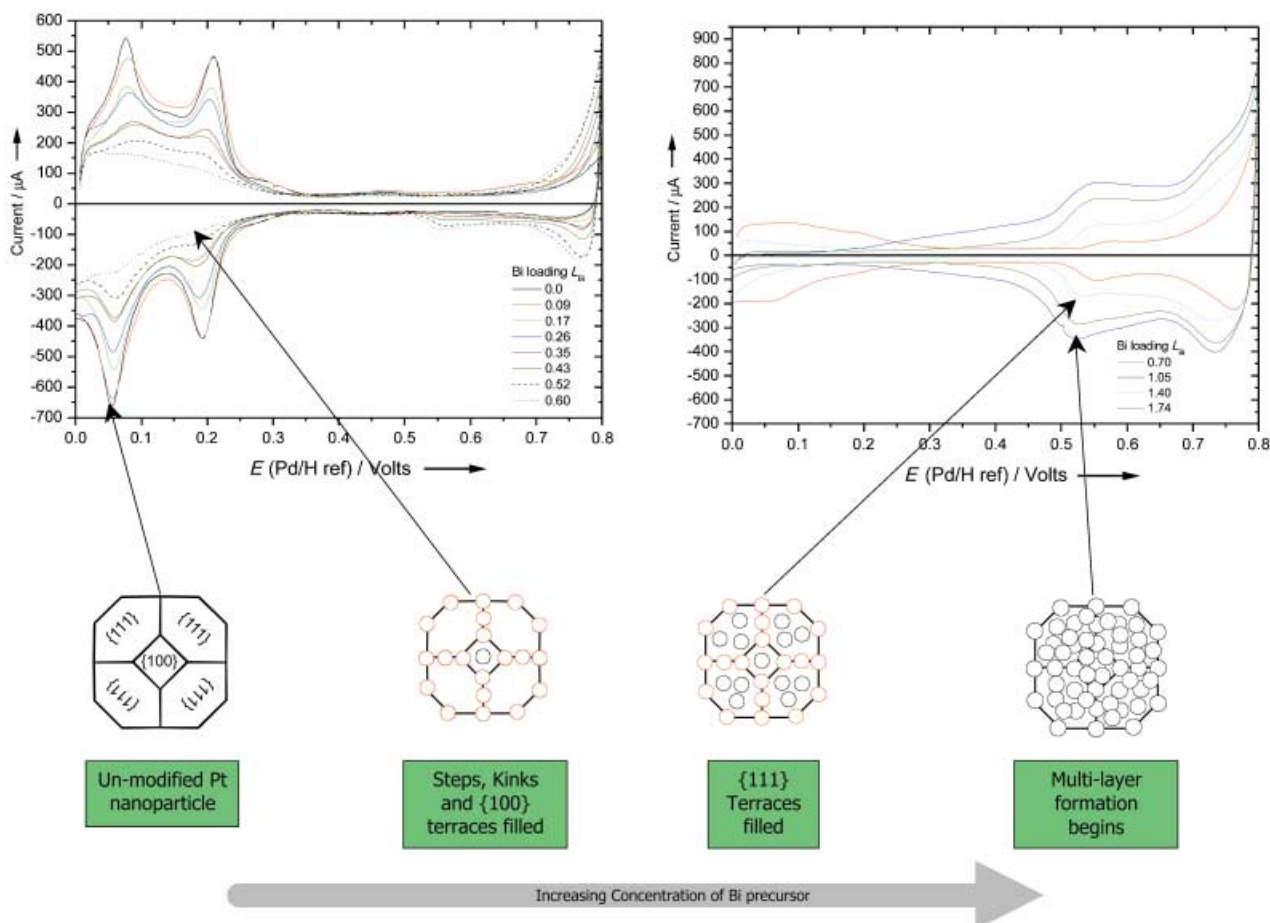


Figure 3. Voltammetric data collected from a 5% Pt/graphite catalyst that has been dosed with increasing amounts of Bi. The bismuth coverage is indicated in terms of free Pt sites and hence a Bi loading $L_{\text{Bi}} = 1$ means full blocking of all Pt electroadsorption sites. It should be noted that, as predicted from Figure 2, at a bismuth loading of 0.5–0.6, although all defect and (100) terrace sites are blocked, (111) terrace sites remain unaffected as signified by the presence of the broad peak between 0.4 and 0.55 V. At bismuth loadings in excess of 0.6, the (111) terrace sites become occupied signified by the emergence of a characteristic surface bismuth redox peak at 0.58 V. A schematic representation of these changes in terms of occupation of various types of site on a cubo-octahedral nanoparticle is also shown.

particles, STM has been used to obtain atomic resolution of the annealed particle edge. It should be noted that, normally, STM imaging of high surface area catalyst powders is not thought to be possible. However we have managed to overcome these difficulties and Figure 5 shows, for the first time, an STM image of the 5% Pt/graphite catalyst at low resolution together with an image of one of the annealed (800 K) platinum nanoparticles at atomic resolution. The adlayer observed is due to an oxygen overlayer that is always present prior to reduction.^[25] Hence it is clear from Figure 5 that a 120° angle is formed between the sides of the particle and that the particles are actually flat rather than cubo-octahedral consisting of perhaps five or six atomic layers. We emphasise the potential of this result at this point. It means that it may be possible to image, at molecular resolution a “real” enantioselective catalyst under ambient reaction conditions whilst simultaneously monitoring the reactant and product distribution. This will be the subject of a future publication.^[26] When these heat-treated catalysts are used as catalysts in the Orito reaction the enantiomeric excess (*e.e.*—a measure of how enantioselective is the catalyst) increases with increasing annealing temperature and passes through a maximum at

700 K (Table 1). A similar result was obtained by Orito and co-workers in their original paper.^[6] Therefore, is it possible to interpret the change in *e.e.* as a function of annealing temperature? Clearly, at high annealing temperatures, larger flat particles are generated and small particles are consumed. Yet the *e.e.* goes through a maximum suggesting that very large particles may not be suitable for enantioselection. As stated previously, chiral kinks appeared not to play a role in enantioselection for platinum single crystal substrates.^[5, 15] However these earlier studies did not address the possibility of either co-adsorption effects or adsorption at the support particle perimeter. Could these sites be chiral?

Figure 6 summarises our previous analysis of why kink sites are chiral in terms of the intersection of three fundamental Miller planes (111), (100) and (110) for face-centred cubic crystals. *R*-kinks consist of a (111)–(100)–(110) clockwise sequence whereas *S*-kinks give rise to an anticlockwise sequence of the same sites.^[2–4, 27, 28] Hence in two dimensions, metal surfaces may be chiral if they contain an excess of such sites. In fact it should be noted that the dimensionality in which an object is considered is absolutely critical in defining whether or not it is chiral. In

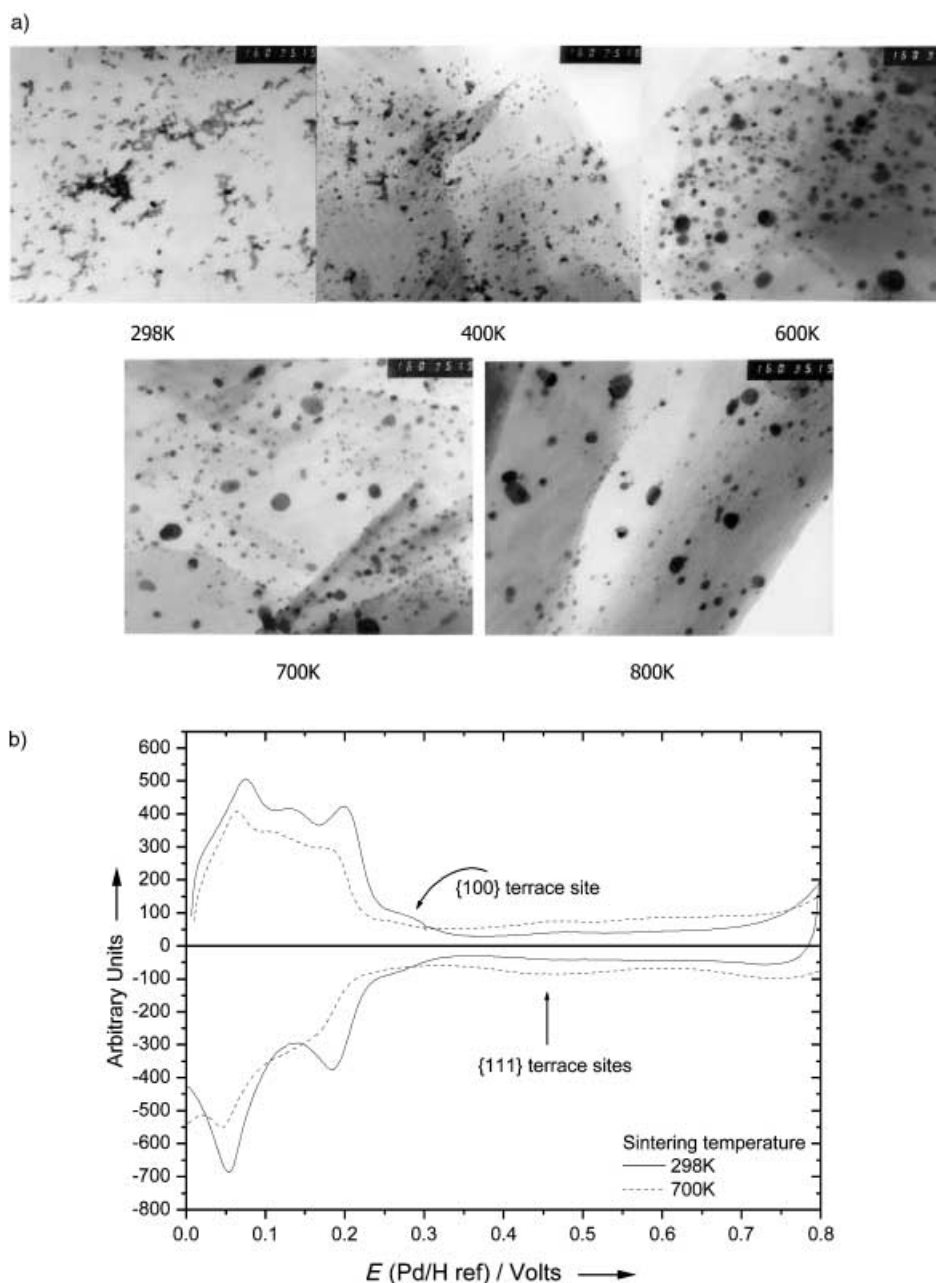


Figure 4. a) Electron micrographs showing changes in particle morphology of a 5% Pt/graphite catalyst upon thermal annealing under argon. In general there is a loss of necking between particles followed by sintering involving the growth of large particles at the expense of the smaller particles. b) These changes are also reflected in CV data collected at 298 K and after annealing at 700 K. The loss of (100) terrace sites and the growth in more extended (111) terrace sites^[19] at high temperature is noted from these voltammetric measurements. Each individual photograph is magnified by $\times 100\,000$.

Figure 7 this point is further emphasised, in that molecules which are thought of as achiral in three dimensions become chiral in two and molecules which are achiral in two dimensions may be considered chiral in one dimension. It is an interesting thought that if one could step outside three dimensions into a fourth, chiral sp^3 carbon atoms should not be chiral! Further discussion of these points may be found in refs. [4] and [29]. Finally in Figure 8 a flat hexagonal nanoparticle is shown in which each corner is assigned as *R* or *S* depending on whether or not the sequence of adsorption sites (111) – (100) – (support) runs

clockwise or anticlockwise. If indeed the chiral symmetry of the particle support edge is important during enantioselection in the Orito reaction, then one may interpret the annealing data as follows.

For small hexagons (Figure 9a), that is, those which are too small to accommodate both chiral modifier and ethyl pyruvate (Etpy) simultaneously at a corner site, enantioselectivity should be low. As the hexagons become larger (Figure 9b), there will be a critical size of particle in which the ensemble of modifier and substrate is present without self-blocking at chiral corners. When

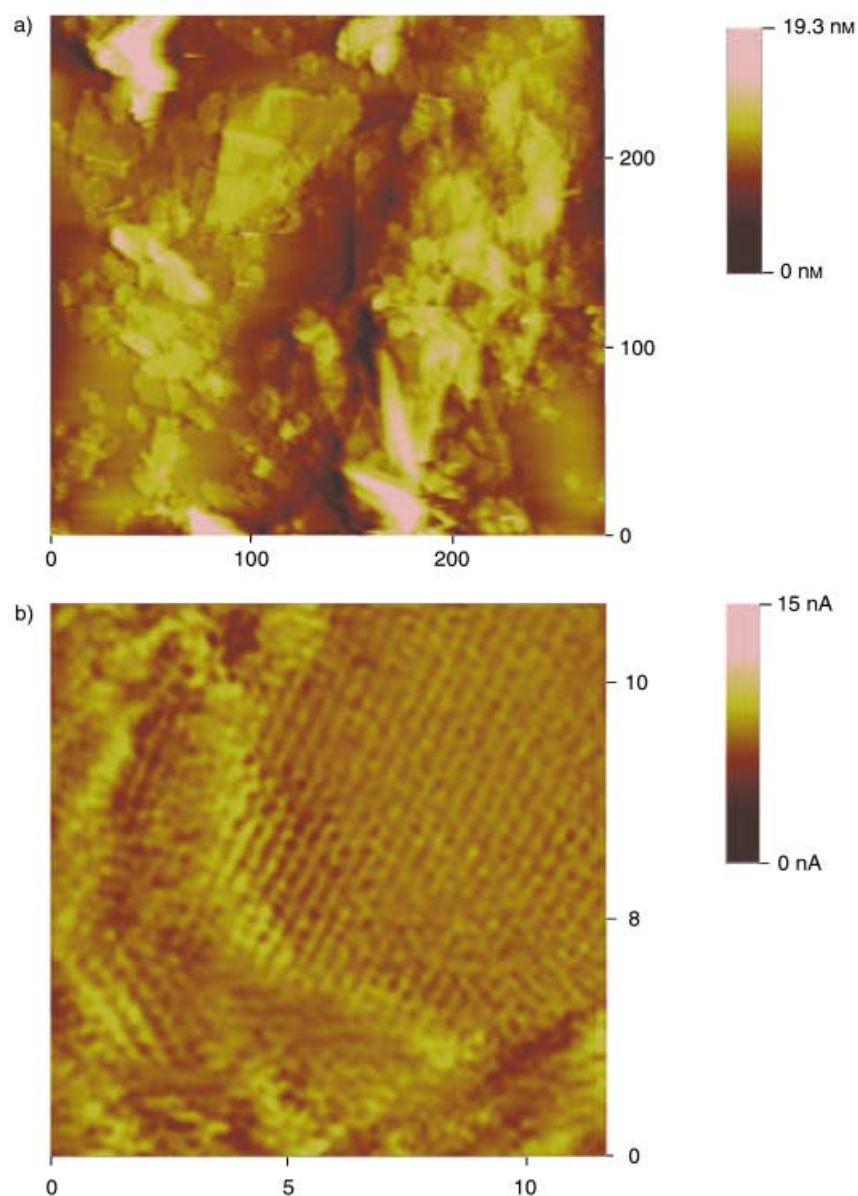


Figure 5. a) STM image of a 5% Pt/graphite catalyst showing the distribution of platinum nanoparticles on the graphite support and b) a magnified image of a nanoparticle from the same catalyst after thermal annealing at 800 K showing straight particle edges. The ordered overlayer of surface oxygen atoms may readily be discerned. All distances are in nanometres.

Annealing temperature [K]	e.e. [%]
298	43
400	49
600	51
700	54
800	48
900	48

the majority of particles are of this form, there will be a maximum in e.e. If however the hexagonal particles grow too large (Figure 9c) then the ratio of racemic sites (steps and

terraces) to corners will start to decrease and so e.e. will also decrease. Even for particles of a size appropriate for enantioselection, *meso*-forms of defect sites^[4] will be present if the edges are either curved or contain *R*- and *S*-sites along the same edge. Presumably it is the annealing out of these sites which causes the e.e. obtained for the unannealed catalyst to increase significantly when straight particle edges become more prevalent. A hypothetical "ideal" supported enantioselective catalyst based on the above would consist of ordered arrays of flat hexagonal platinum particles whose sides were the same size as the diameter of the pyruvate-alkaloid-corner complex and whose separation was typically of a similar magnitude. In fact, EUROPT-1 (a 6.3% Pt/silica catalyst), an excellent catalyst for enantioselective hydrogenation, has been shown to possess many of the attributes discussed here.^[30]

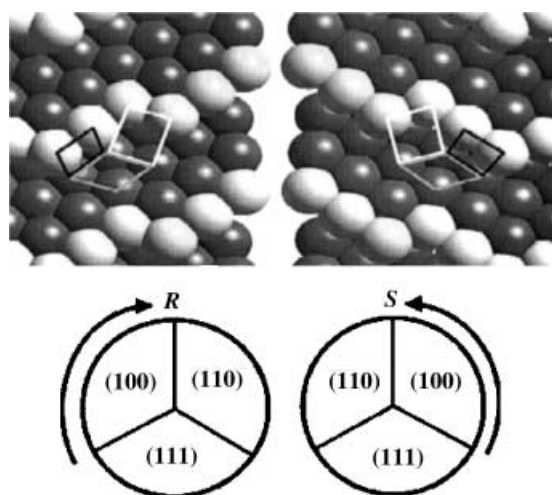


Figure 6. A summary of the analysis used to identify kink sites as being chiral. The edge atoms of a Pt(643) surface are highlighted together with the fundamental (111) (grey), (100) (black) and (110) (white) sites constituting the kink site. It is noted that by taking the sequence of these sites (111)–(100)–(110) that two nonsuperimposable versions of the surface may be generated, designated R or S. This point highlights the importance of considering the dimension in which an object is considered as being chiral.

In conclusion, a new method of characterising the surface morphology of supported platinum nanoparticles is presented based on a combination of voltammetry and STM. The nature of surface chirality in terms of reduced dimensionality has also been addressed and some preliminary data pertaining to surface modifications associated with selective site decoration and thermal treatments discussed. The thermal annealing data would be consistent with a model of enantioselection involving chiral corner sites and hence a speculative “designer catalyst” for heterogeneous enantioselection is proposed which would be suitable for carrying out Orto-type reactions.

Experimental Section

All electrochemical measurements were carried out using water supplied from a three-stage Millipore Milli-Q plus 185 purification system (resistivity $> 18.2 \text{ M}\Omega \text{ cm}^{-1}$) and ultrapure reagents supplied by Sigma–Aldrich. The electrochemical apparatus has been described previously^[21] and all potentials are quoted versus a saturated H/Pd wire in the electrolyte solution. The 5% Pt/graphite catalyst was supplied by Johnson Matthey and corresponded to an average particle size of 4 nm based on dispersion measured via CV and assuming spherical Pt particles. TEM measurements were performed at Hull University by Janice Halder and thermal annealing of the 5% Pt/graphite catalyst carried out in a tube furnace flushed with argon at constant temperature at Johnson Matthey (Royston, UK). All STM measurements were performed at 1 bar nitrogen pressure at 293 K in a Molecular Imaging EC–STM described previously.^[31] All ethyl pyruvate hydrogenations were carried out using 0.25 g of catalyst, 50 mg of cinchonidine, 65 mmol of ethyl pyruvate in 12.5 mL of dichloro-

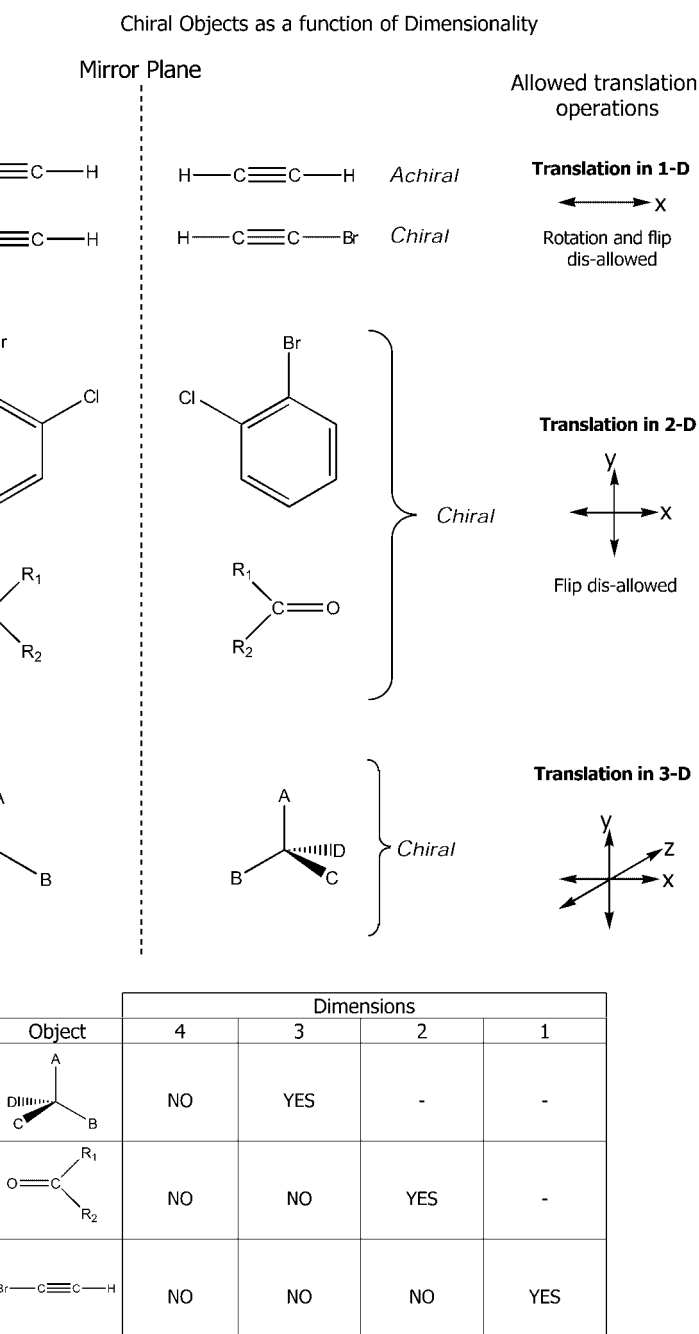


Figure 7. Various examples of chiral and achiral objects as a function of the dimension in which they are contained.

Object	Dimensions			
	4	3	2	1
	NO	YES	-	-
	NO	NO	YES	-
$\text{Br}-\text{C}\equiv\text{C}-\text{H}$	NO	NO	NO	YES

methane at ambient temperature (298 K) and 30 bar of hydrogen pressure with a stirring speed of 1000 rpm.

G.A.A. wishes to acknowledge the EPSRC for a studentship to D.J.J. and a PDRA position to A.A. (grant number M65724). The financial support of Johnson Matthey is also gratefully acknowledged. We thank Dr. David Willock for stimulating discussions during the writing of the manuscript and also for providing several of the ball models used in the figures. O.A.H. acknowledges the financial support of the Saudi Arabian Government.

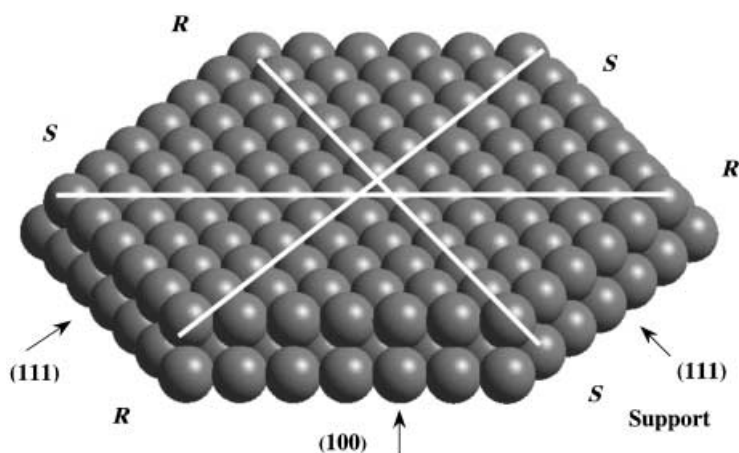


Figure 8. A schematic of a flat hexagonal Pt nanoparticle on a support. Using a similar analysis to that highlighted in Figures 6 but including the support as a distinguishable surface site, it is observed that the corners of the hexagon are chiral with alternating R- and S-sites. If these sites are important for enantioselection during Orito-type reactions, then the size of the "footprint" of the cinchona–pyruvate complex relative to the size of the hexagon is critical. It is predicted that an optimum size of Pt hexagonal platelet is required for enantioselection in which the optimum ratio of corner sites to steps and terraces is achieved.

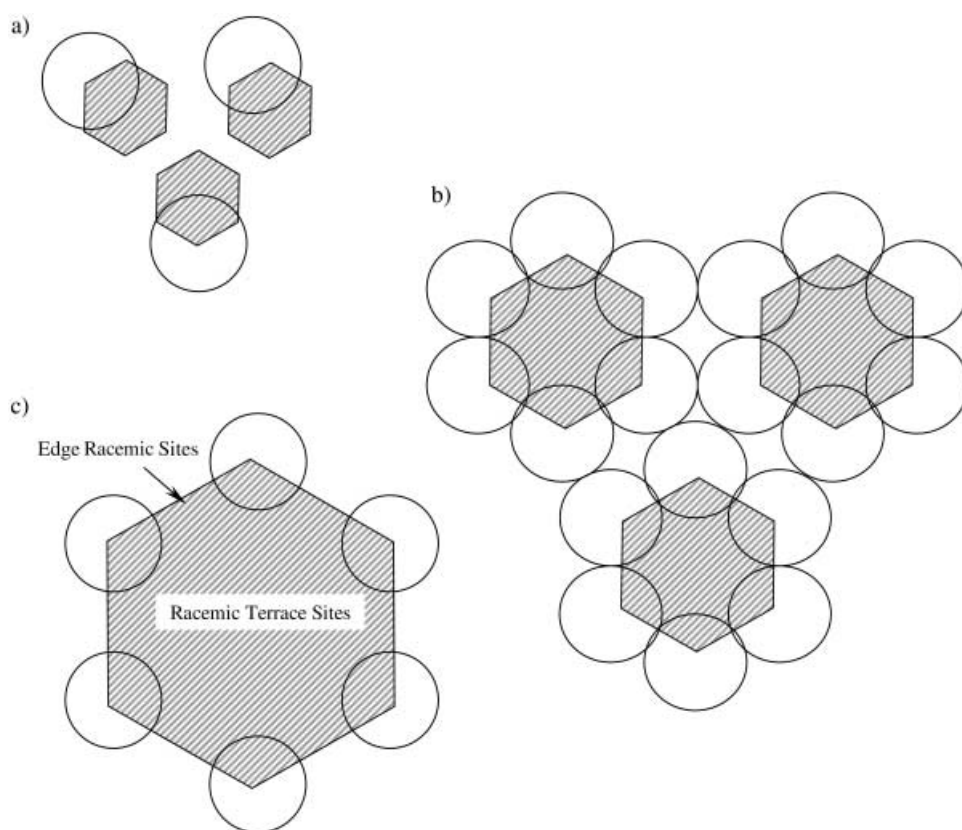


Figure 9. The optimum ratio of corner sites to steps and terraces is shown for an Etpy–cinchona complex (circles) on a hypothetical "designer" catalyst (hexagons) based on previous sintering data (see text). a) For small nanoparticles the complex regions overlap so only partial occupation of the corner sites is possible and a poor e.e. results. b) For an optimised nanoparticle size and distribution, the complexes just fit at all the corners and the e.e. is also optimised. c) For large nanoparticles, although the complexes are accommodated at the corners, there are also more racemic sites (terraces and edges), which leads to a lowering of e.e.

- [1] S. C. Stinson, *Chem. Eng. News* **2000**, *78*, 55.
 [2] A. Ahmadi, G. Attard, J. Feliu, A. Rodes, *Langmuir* **1999**, *15*, 2420.
 [3] G. A. Attard, A. Ahmadi, J. Feliu, A. Rodes, E. Herrero, S. Blais, G. Jerkiewicz, *J. Phys. Chem. B* **1999**, *103*, 1381.
 [4] G. A. Attard, J. Clavilier, J. M. Feliu, in *Chirality: Physical Chemistry* (Ed.: J. M. Hicks), ACS Symp. Ser. 801, ACS Publications, Washington, DC, **2002**, p. 254.
 [5] G. A. Attard, *J. Phys. Chem. B* **2001**, *105*, 3158.
 [6] Y. Orito, S. Imai, S. Niwa, *J. Chem. Soc. Jpn.* **1979**, *8*, 1118.
 [7] A. Baiker, *J. Mol. Catal.* **1997**, *115*, 473.
 [8] H.-U. Blaser, H. P. Jallet, M. Muller, M. Studer, *Catal. Today* **1997**, *37*, 441.
 [9] P. B. Wells, A. G. Wilkinson, *Top. Catal.* **1998**, *5*, 39.
 [10] H.-U. Blaser, *Tetrahedron: Asymmetry* **1992**, *2*, 319.
 [11] I. M. Sutherland, A. Ibbotson, R. B. Moyes, P. B. Wells, *J. Catal.* **1990**, *125*, 77.
 [12] J. L. Margitfalvi, M. Hegedus, *J. Mol. Catal. A: Chem.* **1996**, *107*, 281.
 [13] A. Baiker, T. Burgi, *J. Am. Chem. Soc.* **1998**, *120*, 12920.
 [14] K. E. Simons, P. A. Meheux, S. P. Griffiths, I. M. Sutherland, P. Johnston, P. B. Wells, A. F. Carley, M. K. Rajumon, M. W. Roberts, A. Ibbotson, *Rec. Trav. Chem. Pay-Bas* **1994**, *113*, 465.
 [15] M. J. Stephenson, R. M. Lambert, *J. Phys. Chem. B* **2001**, *105*, 12832.
 [16] M. von Arx, A. Baiker, *Top. Catal.* **2002**, *19*, 75.
 [17] F. Zaera, A. J. Gellman, G. A. Somorjai, *Acc. Chem. Res.* **1986**, *19*, 24.
 [18] See for example: "Frontiers in Surface and Interface Science" (Eds.: C. B. Duke, W. Plummer) *Surf. Sci.* **2002**, 500.
 [19] *Interfacial Electrochemistry* (Ed.: A. Wieckowski), Marcel Dekker, New York, NY, **1999**.
 [20] J. Clavilier, J. M. Feliu, A. Aldaz, *J. Electroanal. Chem.* **1988**, *243*, 419.
 [21] R. W. Evans, G. A. Attard, *J. Electroanal. Chem.* **1992**, *345*, 337.
 [22] J. M. Feliu, A. Fernandez-Vega, A. Aldaz, J. Clavilier, *J. Electroanal. Chem.* **1988**, *256*, 149.
 [23] E. Herrero, V. Climent, J. M. Feliu, *Electrochem. Comm.* **2000**, *2*, 636.
 [24] J. M. Feliu, M. J. Llorca, R. Gomez, A. Aldaz, *Surf. Sci.* **1993**, *297*, 209.
 [25] G. A. Attard, J. E. Gillies, C. A. Harris, D. J. Jenkins, P. Johnston, M. A. Price, D. J. Watson, P. B. Wells, *Appl. Catal. A* **2001**, *222*, 393.
 [26] A. Ahmadi, G. A. Attard, unpublished results.
 [27] C. F. McFadden, P. S. Cremer, A. J. Gellman, *Langmuir* **1999**, *12*, 2483.
 [28] T. Power, D. S. Sholl, *Top. Catal.* **2002**, *18*, 201.
 [29] Q. Chen, D. J. Frenkel, N. V. Richardson, *Surf. Sci.* **2002**, *497*, 37.
 [30] J. W. Geus, P. B. Wells, *Appl. Catal.* **1985**, *18*, 231.
 [31] G. A. Attard, C. J. Barnes, M. R. Smyth, C. M. Whelan, *J. Electroanal. Chem.* **1999**, *474*, 138.

Received: August 21, 2002 [C 490]